CHROMOSPHERIC OSCILLATIONS

R.J. Rutten

Sterrekundig Instituut, Postbus 80 000, NL–3508 TA Utrecht, The Netherlands; rrutten@solar.stanford.edu

ABSTRACT

This review concentrates on the quiet-Sun chromosphere. Its internetwork areas are dynamically dominated by the so-called chromospheric three-minute oscillation. They are interpretationally dominated by the so-called Ca II K_{2V} and H_{2V} grains. The main points of this review are that the one phenomenon explains the other (both ways), that the quiet-Sun chromosphere is a *clapotisphere* pervaded by shocks above $h \approx 1$ Mm, and that the existence of the classical temperature minimum is in doubt.

Keywords: solar oscillations, chromosphere, clapotisphere.

1. INTRODUCTION

Twenty years ago helioseismology was founded by the identification of the photospheric five-minute oscillation as the surface interference pattern of millions of solar p modes. The identification came about as synthesis between observed and computed Ulrich ridges [1] in the (k, ω) diagram [2].

A comparable synthesis between observations and computations is now taking place for the three-minute chromospheric oscillation, a quiet-Sun internetwork phenomenon, with the temporal spectral variations of the so-called Ca II H_{2V} and K_{2V} as decisive diagnostic. The synthesis indicates that:

- the grains are of oscillatory nature;
- the oscillations are driven from the photosphere, with (k, ω) ridge structure imposed by the piston;
- the internetwork chromosphere is far from hydrostatic equilibrium. Its line formation is dominated by shock interference that upsets plane-parallel height-of-formation interpretation;
- the mean internetwork chromosphere is cool but radiates in the ultraviolet as if it were hot;
- infrared CO lines share in chromospheric behavior without special distinction.

Since this paper is a review, it describes much work by others; since it has a page limit, it does not do justice to much work by other others. More complete descriptions and references are given in [3], [4]. The latter review is part of the highly recommended 1994 Oslo Miniworkshop proceedings [5] of which this paper presents a summary.

2. THREE DECADES OF POWER SPECTRA

The chromospheric internetwork oscillations have been known nearly a century in their Ca II K_{2V} grain disguise. Fourier analysis started at Mount Wilson in the sixties, just as for the five-minute oscillation. Noyes' [6] classic diagram in Fig. 1 exhibits the characteristic power progression with height, from low-frequency intensity modulation by granulation at the bottom of the photosphere (bottom graph) through dominance of the five-minute p–modes in the photosphere (C I and Fe I Dopplershifts) to a wide peak roughly centered at three minutes for Ca II K. The diagram demonstrates that the "chromospheric three-minute oscillation" is not exclusively chromospheric nor exclusively three-minute, facts often forgotten. Rather, the balance of dynamical power shifts with height from granulation to five-minute modes to higher-frequency fluctuations. At any height there is much overlap, which needs to be disentangled.

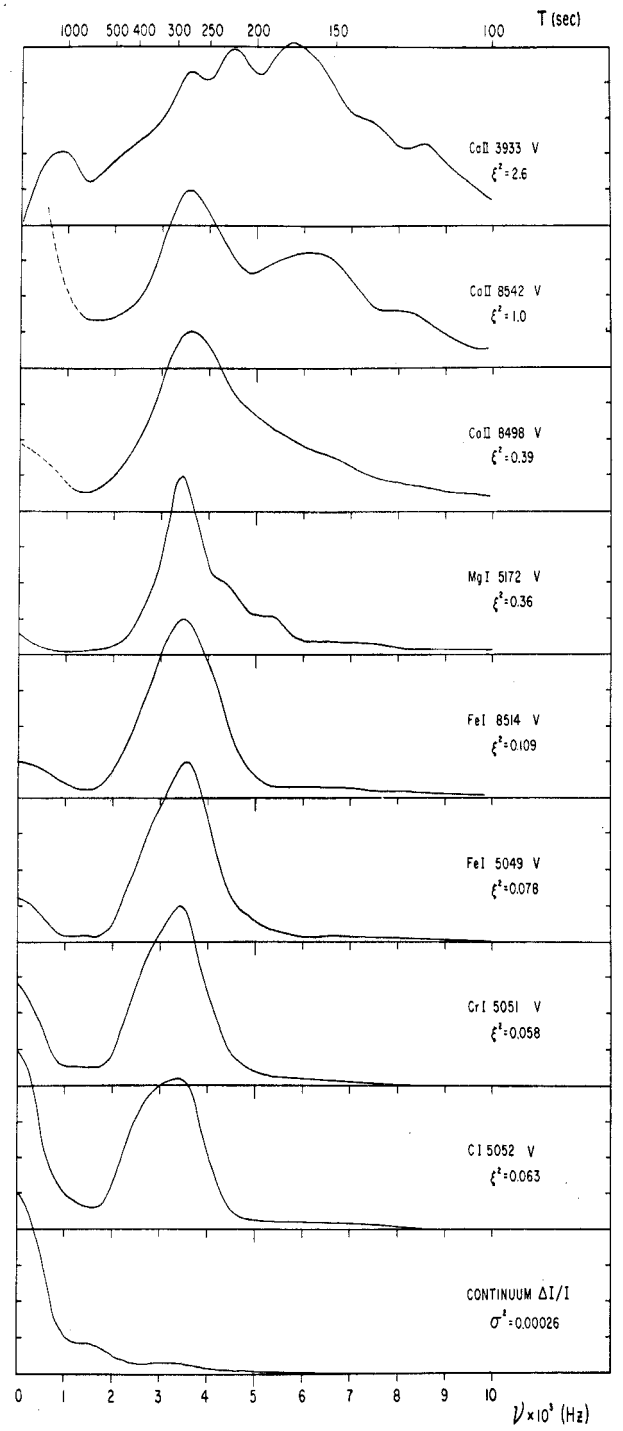

Figure 1: Normalized power spectra anno 1967. The bottom spectrum is for continuum intensity fluctuations. The other spectra are for Dopplershift variations of the indicated lines. They range from the deep photosphere (C I) to the middle chromosphere (Ca II K, top). The parameter $\xi = 1.4\, v_{\rm rms}\,{\rm km\ s^{-1}}$. From Noyes [6].

Figure 2 is from Cram's underquoted 1978 paper [7]. It shows a similar progression in reversed panel ordering. The blob of velocity power in these quasi-diagnostic dia-

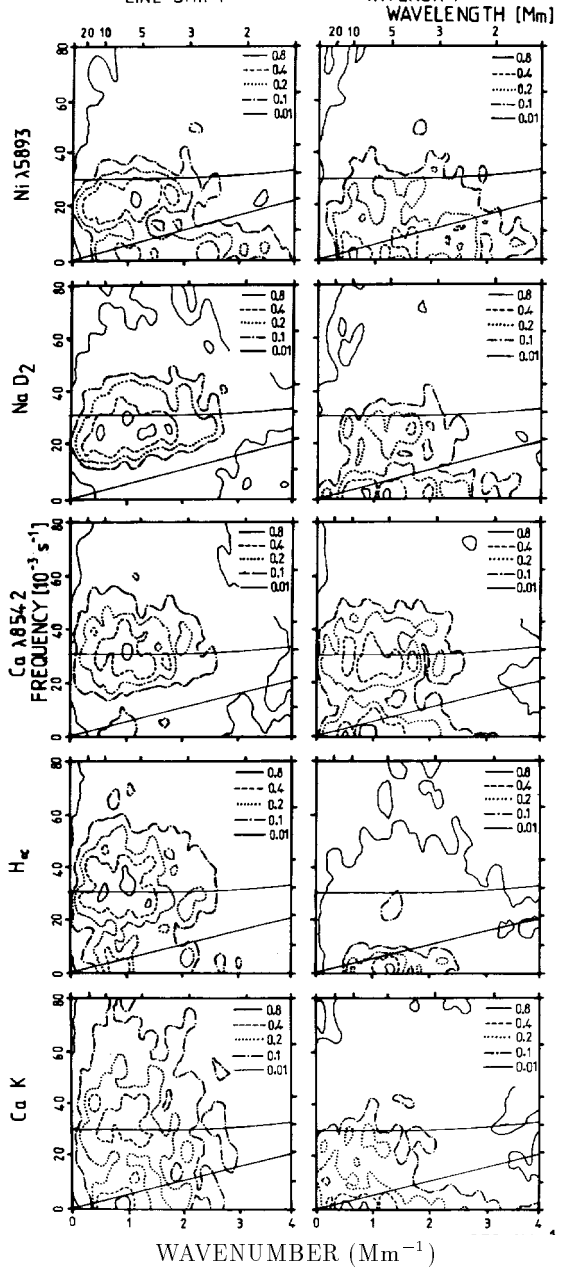

Figure 2: Diagnostic $\nu - k_h$ power diagrams anno 1978 for velocity and intensity fluctuations of the lines indicated at left, based on one-dimensional HIRKHAD slit spectrometry. The spatial decomposition assumed circular symmetry on the solar surface. The solid curves separate the acoustic (top part of diagram), evanescent (middle) and gravity (bottom) regimes for a 5000 K atmosphere. Cram's paper contains also $V - I$ phase difference and coherence spectra for these and other diagnostics. From Cram [7].

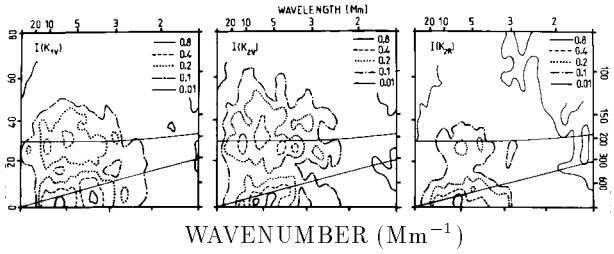

Figure 3: Diagnostic $\nu - k_h$ power diagrams anno 1978 for intensity fluctuations of Ca II K features, respectively the the K_{1V} blueward dip, the K_{2V} blue peak, and the K_{2R} red peak of the spatially-averaged profile. The line-center K_3 variations are shown in Fig. 3. From [7].

line formation. The intensity blob at right lags behind. For example, Na I D I resembles Ni I V, illustrating that scattering lines have deeper response for intensity than for velocity fluctuations. Higher up, Hα and Ca II K share abruptly different behavior: the velocity blob is present and extends well into the propagating regime, but the intensity blob vanishes. This behavior demonstrates that something drastic happens to the intensity modulation at the formation height of these lines. In addition, low-frequency modulation appears significant in the higher-formed intensity signals. Spatially, the power occupies a fairly wide range (2–10 Mm) around wavelength $\Lambda \approx 8$ Mm at all formation heights.

Figure 3 shows similar Cram diagrams for Ca II K features. The K_{1V} dip (left panel) resembles Ca II 8542 I behavior. The K_{2R} peak (right) resembles K_3 I, but K_{2V} (middle) is closest to Hα V. Later work has shown that the intensity ratio $(K_{2R} - K_{2V})/(K_{2R} + K_{2V})$ is a close proxy for K_3 Dopplershift [8]. Thus, the Ca II K core lacks line-formation symmetry; the intensity at the wavelength of the blue K_{2V} peak is primarily a velocity diagnostic.

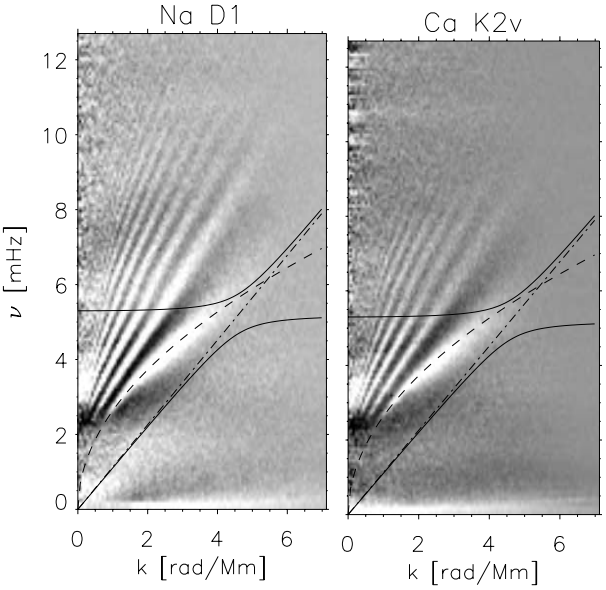

Figure 4: Diagnostic $\nu - k_h$ power diagrams anno 1994 for intensity fluctuations of Na I D_1 and Ca II K_{2V}. The solid curves again divide the three wave regimes. The dashed curves define the Lamb and fundamental modes. The structure in both diagrams has been enhanced by subtracting smooth background variations. After [9], by courtesy of Bernhard Fleck.

Finally, Fig. 4 shows the present state of the art. These Würzburg productions for Na I D_1 and Ca II K_{2V} I fluctuations resolve Cram's blobs into Ulrich p–mode ridges and pseudo-mode ridges higher up. The latter were earlier noted by Kneer & von Uexküll [10] and extend out to $k_h \approx 5$ rad/Mm and to $\nu \approx 11$ mHz in Na I D_1 and $\nu \approx 9$ mHz in K_{2V}. Weak interridge power is present particularly near $\nu = 6$ mHz [11], [12].

3. NETWORK—INTERNETWORK

Cram's diagrams in Figs. 2–3 provide a neat summary of much of the subsequent chromospheric dynamics literature. However, they do not distinguish between network and internetwork; his slit sampled internetwork area primarily [14]. Figure 5 illustrates that such separation is necessary at chromospheric heights. The bottom panel shows photospheric p–mode power without network/internetwork difference but the middle panel

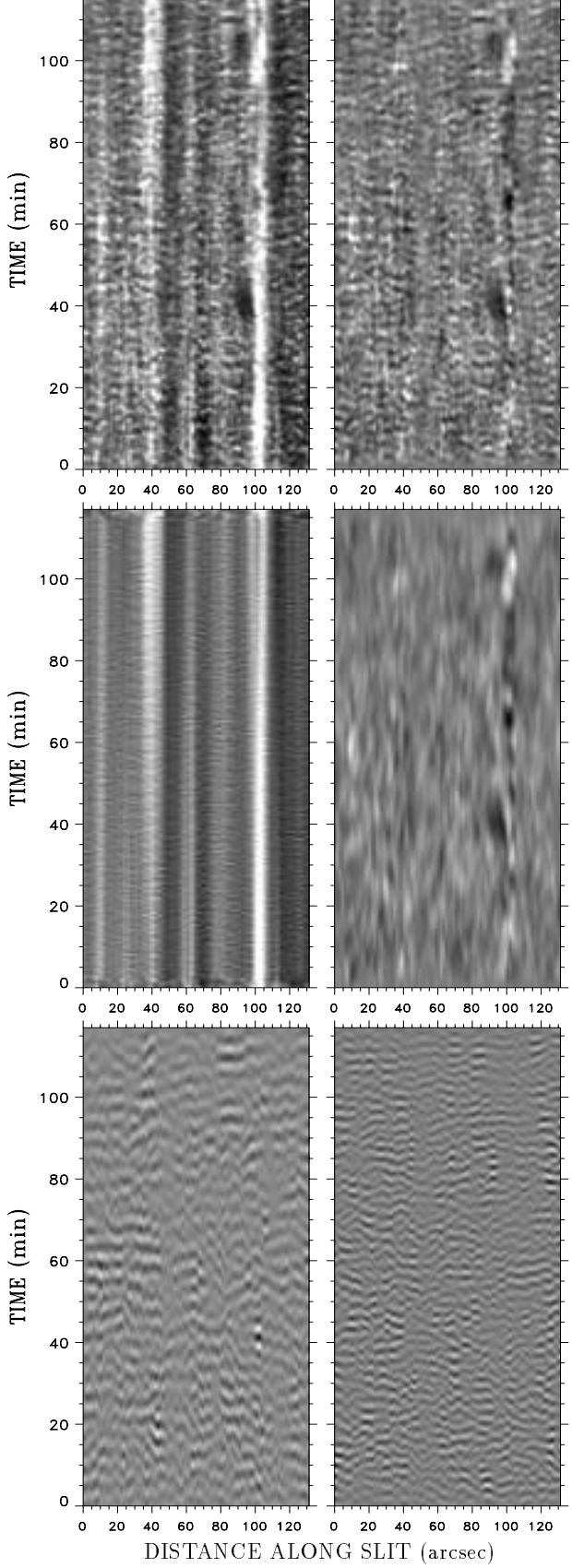

Figure 5: Network and internetwork velocity power in the chromosphere (middle panel, Ca II H) and photosphere (bottom panel, Fe I 3966.82). Larger power is grey-scale coded as darker. The column near $x = 30$ Mm in the middle panel is due to seeing jitter of a small network feature across the slit. The top panel shows time-averaged spectral profiles of the Ca II H core per pixel along the slit. The chromospheric network is marked by bright H_{2V} and H_{2R} emission around $x = 30$ Mm. This location has markedly different power distribution in the Ca II panel. From [13].

for Ca II K_3 V fluctuations displays marked difference between the internetwork three-minute oscillations, extending from 3 to 10 mHz, and the network fluctuations, which have much slower periodicities. The latter are not understood. They may depict stochastic granular rearrangement of network fluxtubes [15] or oscillatory phenomena such as breaking gravity waves [13], [16]. They aren't discussed here any further, but they do need further scrutiny.

4. Ca II K_{2V} GRAINS

K_{2V} internetwork grains on spectroheliograms were first described and shown by Hale & Ellerman [17]. They are small (0.5–1.5 Mm), short-lived (30–100 s), come and go with 2–5 min intervals, and appear to be distributed in 2–10 Mm patterns in network cell interiors. On K_{2V} movies they are seen to be part ("the tip of the iceberg") of spidery, rapidly changing structures with often large (50–100 km s^{-1}) apparent horizontal velocities. They appear very much as the whitecaps seen on the Atlantic from your plane flying to meetings as this one. They are spectrally confined to the narrow K_{2V} peak location, but they take part in the temporal behavior of wider surroundings both spectrally and spatially [18]. A matter of debate is whether the grains mark sites of enhanced internetwork field as claimed by Sivaraman [19], [20]. More detail is given in [3], [21], [10], [4], [22], [23], [12].

The upper-left panel in Fig. 6 illustrates temporal K_{2V}

Figure 6: Fourier-filtered time slices. The top-left panel is a two-hour time-slice plotting H_{2V} intensity evolution per pixel along the slit as grey scale. The other panels show the same data after temporal filtering per column. Top right: sum of long-period, five-minute and three-minute bands. Middle left: leftover (sum of lowest and highest frequencies). Middle right: long-period band. Bottom left: five-minute band. Bottom right: three-minute band. From data of [8], reduced by B.W. Lites.

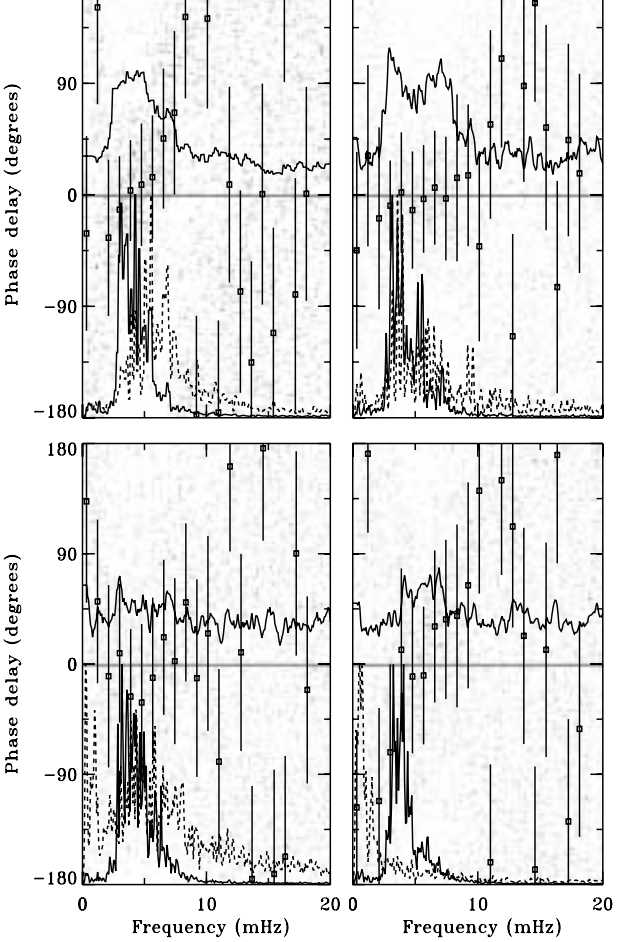

Figure 7: Phase difference spectra between Al I 3961.54 and Ca II H_3 Dopplershifts, computed following [13]. Positive phase delay implies upward propagation in the acoustic regime. The grey-scaled dots mark amplitude-weighted phase difference per temporal frequency and per spatial position along the slit. The squares are their average per frequency bin, with rms bars. The curve in the upper half of each panel is the coherency, scaled 0–1 and determined by 9-point frequency smoothing. The lower pairs of curves are normalized power spectra, solid for Al I and dashed for H_3. Upper-left panel: slit positions 116–131″ with many H_{2V} grains (Fig. 6). Upper right: 6–15″ with "persistent flasher". Lower left: dark region at 46–57″. Lower right: network at 93–106″. Copied from [4]; produced by B.W. Lites from data of [8].

characteristics from NSO/Sacramento Peak spectrometry. The chromospheric network stands out as bright striping. H_{2V} grains are seen as short-lived and small-scale brightness features in internetwork areas, especially on the right. The other panels are Fourier-filtered displays of the same data. They show that the grains are made up by combinations of long-period, five-minute and three-minute modulations. The latter have the largest weight in setting grain appearance, but display wavy-curtain patterning that is similar to the *p*–mode interference patterns in the five-minute panel. The temporal periodocities are of course smaller in the righthand panel, but the morphology is qualitatively similar.

Solar oscillations are traditionally diagnosed from phase difference and coherency spectra between various diagnostics. This tactic is employed in the four Bruce Lites confusograms in Fig. 7, with separation between various regions along the slit that are distinct in Fig. 6. The limited spatial sampling increases the scatter but the spatial separation is clearly warranted by the resulting differences. The grainy area seen at right in the upper-left

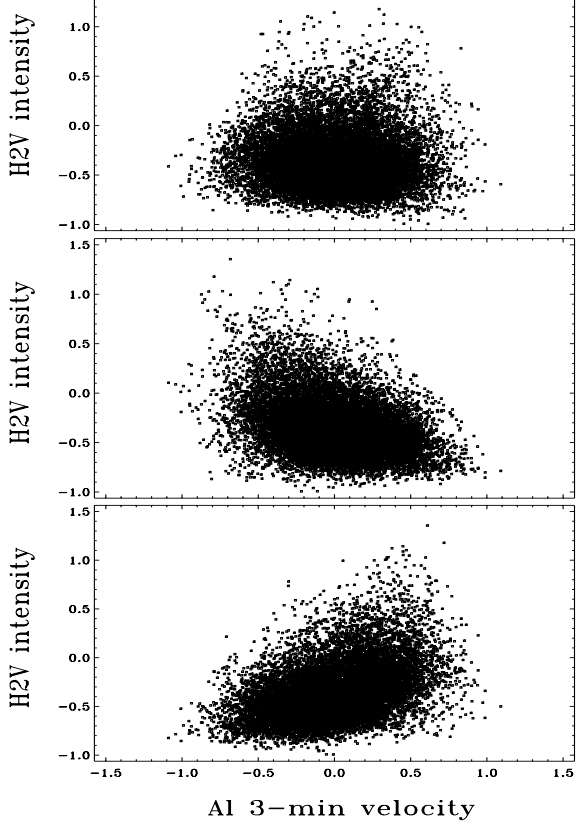

Figure 8: H_{2V} intensity per time-slice pixel against the three-minute component of Al I 3961.54 Dopplershift at different time delays, for the grain-rich 116–131″ segment in Fig. 6. Velocities in km s^{-1} with blueshift positive; intensities in arbitrary units around the spatial mean. Top: simultaneous sampling. Middle: Al I velocity sampled one minute before H_{2V} intensity. Bottom: two minutes delay. From [4].

panel of Fig. 6 contains increasing upward propagation over the 5–10 mHz band (upper-left panel of Fig. 7). The upper-right panel is for a small area with many grains superimposed on network-like striping. Its phase delay is close to zero throughout the region with high coherence. The lower-left panel is for a dark strip without grains and is mostly noisy. The lower-right panel is characteristic for network behavior. A slightly more extended discussion is given in [4].

The next step is to study phase relationships specifically for the brightest H_{2V} grains. This is done in Fig. 8 by sacrificing frequency resolution for intensity characteristics. The leftward and rightward tilting of the scatter clouds in the two delay plots show that K_{2V} intensity tends to follow three-minute Al I velocity modulation, another way of depicting the upward propagation. The grains take part in this correlation: the brightest H_{2V} samples also tend to follow one minute after Al I redshift and two minutes after Al I blueshift. Thus, K_{2V} grains are part of the oscillations diagnosed in Figs. 1–7.

5. NUMERICAL SIMULATIONS

The displays above establish that Ca II K_{2V} grains are part of oscillatory phenomena in the acoustic regime. That makes them amenable to numerical simulation. The development of numerical wave modeling has gone from early scenario's [25] – [27] and simulation [28], [29] through identification of the underlying principles [30] – [34] to detailed modeling [35] – [37] that has now reached realistic reproduction of many observed properties by Carlsson & Stein [24]. In this section I summarize some

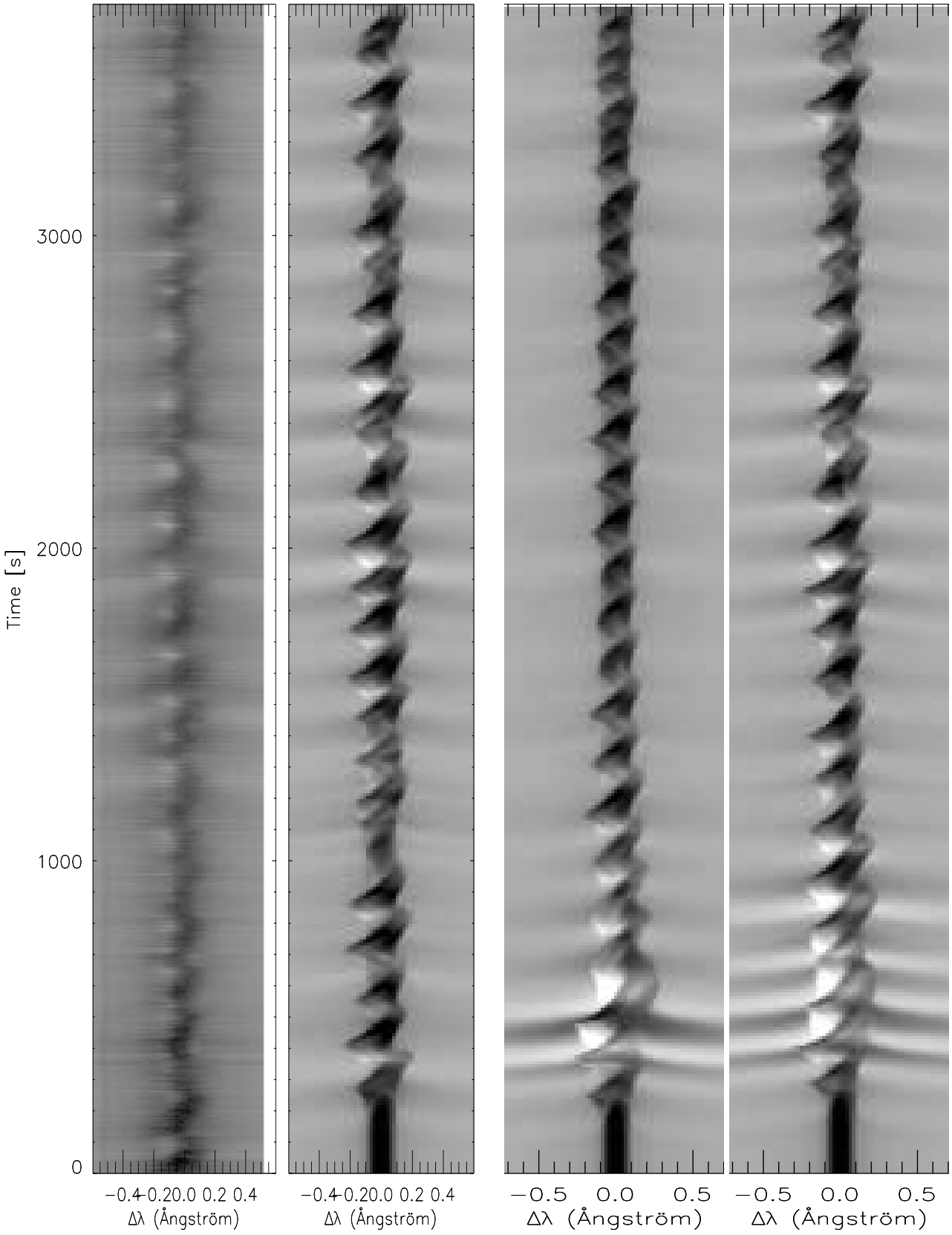

Figure 9: Observed and computed CaII H spectral evolution diagrams. First column: observed intensity behavior from [13]. Second column: numerical modeling by Carlsson & Stein, using a subphotospheric piston that reproduces the observed photospheric excursions for the same surface location in the data of [13]. This one-hour simulation took 50 hours CRAY supercomputer time. Third column: simulation result when the piston retains only frequencies below 4.5 mHz. Fourth column: simulation result for piston frequencies above 4.5 mHz. From [24].

the older work.

Carlsson & Stein (abbreviated to CS henceforth[1]) solve the one-dimensional hydrodynamics equations time-dependently for a stratified solar atmosphere including detailed NLTE radiative transfer. There are shortcomings, most notably the use of microturbulence ($2\,\mathrm{km\,s^{-1}}$), the neglect of line blanketing and the assumption of complete frequency redistribution, but the CS hydrogen and calcium NLTE radiative transfer modeling is of unprecendented sophistication. In addition, CS don't employ a sinusoidal or otherwise ad-hoc imposed piston to send waves into the atmosphere. Instead, they use a many-frequency piston derived from actual observations, namely from the Doppler excursions of the Fe I line for which the observed power spectra are shown in Fig. 5. This line is present as a far-wing blend in the Ca II H spectra of [13] and is formed about 100 km above $\tau_{500} = 1$. CS transformed its observed Dopplershift variation at a selected pixel along the slit into subphotospheric piston motion by determining a frequency-dependent transfer function that makes the piston generate the observed velocity variation at $h = 100$ km. The question is then whether the computed behavior of the chromosphere resembles the observed behavior.

The effect of the pistoning on the higher layers is shown in Fig. 9 in the form of Ca II H spectral development diagrams, an excellent way of displaying K_{2V} grain behavior pioneered in the beautiful paper of Cram & Damé [18]. The leftmost column shows the Lites *et al.* [13] observation. The second column shows the CS simulation for the same solar surface pixel. The computation is "sharper" since it is not affected by atmospheric seeing. After the startup period, the observation and computation are remarkably similar in their major characteristics, and even in detail. Thus, feeding the CS radiation hydrodynamics code with a photospheric piston from the Lites *et al.* data produces computed chromospheric Ca II H behavior much like the corresponding observed behavior. In particular, the computation reproduces the wing whiskers [38] and their apparent contraction, the sawtooth pattern of H_3 Dopplershifts with rapid blueward and slower redward excursions, and the occurrence of bright H_{2V} grains at roughly three-minute periodicity. The simulated grains come at about the same moments as the observed ones (a 22 s phase shift is due to piston inadequacy), and there is similar alternation between sequences of bright and less bright grains. These patterns are so detailed that the good correspondence implies that the modeling is essentially correct — the more so since all earlier attempts in K_{2V} grain emulation have failed, see [3]. The correspondence gets even beter when CS mimic atmospheric seeing by smearing and random-perturbation of their result [24].

At the start, the correspondence fails for about five minutes. The computation started from a stably stratified radiative-equilibrium atmosphere; it takes time for the piston to change that unrealistic configuration into the proper state of turmoil. In a second experiment (their Fig. 15), CS restarted the piston an hour later all over again, now using the atmosphere as it was after an hour of mistreatment. After 1000 s, a moment at which the atmosphere is relatively quiescent, both runs are nearly identical. Thus, it takes the piston 5–15 min to establish the upper atmosphere into a pattern that is fully set by the piston history and not by the previous atmosphere history. The grain patterns are set by the piston, not instantaneously but over extended time.

In another experiment, CS studied the response to the piston frequencies. The third column in Fig. 9 is the response to only the low frequencies of the original piston. The fourth coumn is from the reverse case with only the high piston frequencies retained. Comparison with the original result in the second column shows that the high-frequency piston components are the more important pattern contributor, but that modulation by the low frequency components is part of grain production, just as in Fig. 6. During the first twenty minutes, the interference is destructive.

[1] Not *Cum Suis* this time (with apology to Mr. C.).

6. GRAIN FORMATION

The nice thing about Ca II K_{2V} grains that originate in a computer is that their characteristics may be analyzed in detail. CS supply a sequence of informative line formation diagrams in [24] of which Fig. 10 is a specimen for $t = 670$ s (second column in Fig. 9).

The computed intensity profile is shown in the top panel of Fig. 10 (lower curve) on a Dopplershift scale (blueshift positive). It has a prominent H_{2V} grain at $\Delta\nu = 9\,\mathrm{km\,s^{-1}}$. The grey scaling of this panel shows the value of the intensity contribution function $C_I(\Delta\nu, z) \equiv \mathrm{d}I/\mathrm{d}z$. The grain originates from $h = 1.0$ Mm (bright blob). At that height, the velocity (jagged curve at center, shown in all panels) has a $4\,\mathrm{km\,s^{-1}}$ peak that marks an upward travelling disturbance. Higher up, such waves have steepened into shocks that run into back-falling matter from earlier shock passages; the matter just above $h = 1.4$ Mm comes down at $10\,\mathrm{km\,s^{-1}}$.

The other three panels portray the breakdown

$$\begin{aligned} C_I &= \frac{\mathrm{d}}{\mathrm{d}z}\int_0^\infty j_\nu\, \mathrm{e}^{-\tau_\nu}\, \mathrm{d}z \\ &= \kappa_\nu S_\nu\, \mathrm{e}^{-\tau_\nu} \\ &= [S_\nu]\ \left[\tau_\nu\, \mathrm{e}^{-\tau_\nu}\right]\ \left[\frac{\mathrm{d}\ln\tau_\nu}{\mathrm{d}z}\right] \end{aligned}$$

with j_ν the volume emission coefficient, κ_ν the volume extinction coefficient, and S_ν the total source function. The latter is shown by the dashed curve and the grey scaling in the second panel. It follows the Planck function B_ν (dotted curve) in deep layers (bright band), but it drops away from B_ν above $h = 0.8$ Mm due to NLTE scattering. The latter smoothes the response of S_ν to the large temperature contrasts across the shocks considerably. Only the lowest disturbance at $h = 1.0$ Mm leaves a marked S_ν increase, shown as the bright bar. It is constant across the panel because the simulation assumes complete redistribution over the line profile while the continuum contribution to S_ν is negligible at this height.

The factor $\tau_\nu \exp(-\tau_\nu)$ in the third panel peaks around $\tau_\nu = 1$. The latter heights are marked by the dark curve at the center of the bright strip, also shown in the other panels. This factor selects the profile formation height. The damping wings set in at $\Delta\nu = \pm 10\,\mathrm{km\,s^{-1}}$. The core part is strongly affected by the shocks and changes much with time. The steep drop around $\Delta\nu = 10\,\mathrm{km\,s^{-1}}$ at this particular moment results from the large velocity change at $h = 1.4$ Mm. Above this height, the redshifted line-center extinction produces opacity up to $\tau_\nu = 1$ out to $\Delta\nu \approx -10\,\mathrm{km\,s^{-1}}$. No further opacity is added in the first 500 km below this height because there this part of the profile sits well outside the Doppler core. Thus, this part of the profile "is formed" over the extended range $h = 0.6 - 1.6$ Mm without any height discrimination. In contrast, the $\tau_\nu \exp(-\tau_\nu)$ weighting function peaks sharply at the grain-formation height in the left-hand side of the panel.

The bottom panel of Fig. 10 shows the opacity scaling factor $\mathrm{d}(\ln\tau_\nu)/\mathrm{d}z = \kappa_\nu/\tau_\nu$. This factor is large at frequencies and heights with much extinction at small optical

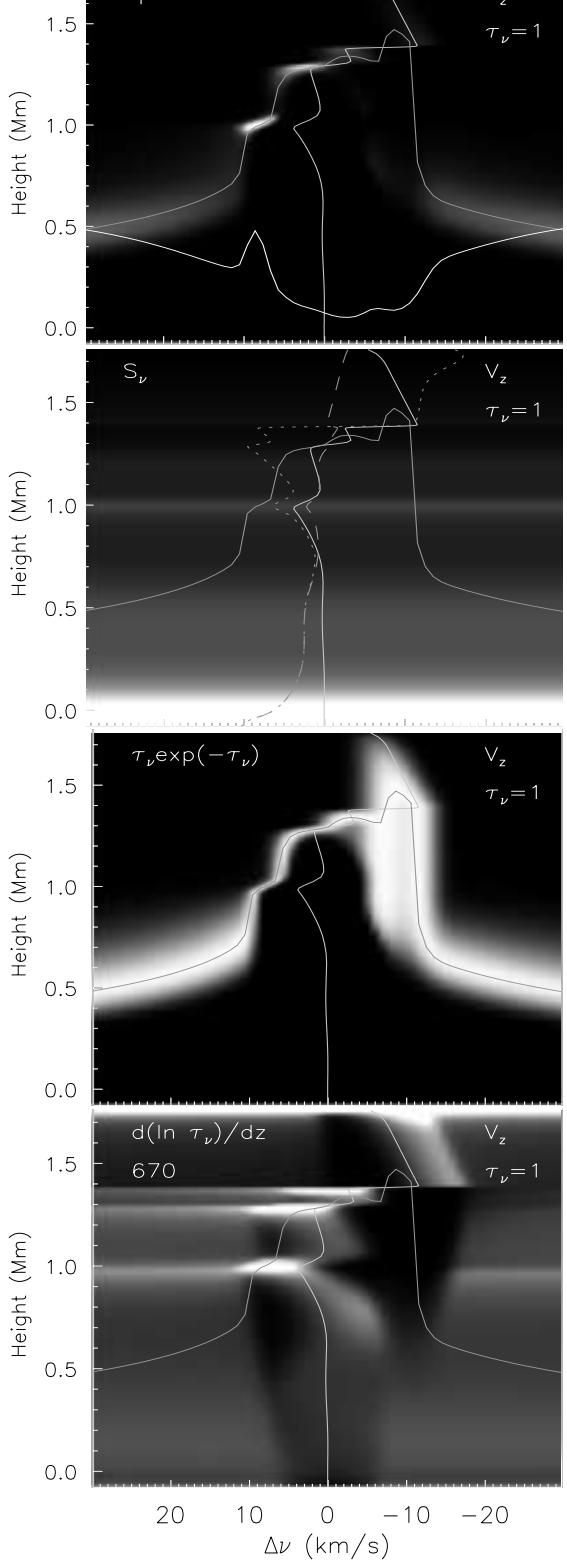

Figure 10: Ca II H line formation diagram for $t = 670$ s. Top: intensity contribution function C_I (brightness coded), emergent profile (lower curve), vertical velocity v_z (jagged curve in the middle), and $\tau_\nu = 1$ height. The latter two curves are also shown in the other panels, which represent a breakdown of C_I into the three brightness-coded factors indicated at the upper left in each panel. From [24].

depth. It peaks in opaque layers for which the overlying matter contributes little opacity, *i.e.*, at the heights of abrupt velocity change where the line-center extinction Doppler-shifts into a fresh region on the way in. It is core has shifted to other frequencies while the overlying matter is opaque. This factor is the main producer of line-profile asymmetry. At $h = 1.0$ Mm the local extinction κ_ν peaks at $\Delta\nu = 4\,\mathrm{km\,s^{-1}}$ Dopplershift (velocity curve), but the steep gradient $\mathrm{d}\tau_\nu/\mathrm{d}\nu$ at this height skews this weighting factor into a brightness blob centered at $8\,\mathrm{km\,s^{-1}}$. Its apparent blueshift is increased by the presence of slower-moving material just above it. This blob, multiplied with the factors in the other two panels, produces the H_{2V} grain at apparent $\Delta\nu = 9\,\mathrm{km\,s^{-1}}$ in the emergent intensity profile. It wins from the other blobs in the upper-left panel by the S_ν multiplication, and it is narrowed in $\Delta\nu$ by the $\tau_\nu \exp(-\tau_\nu)$ formation height factor.

Figure 10 shows that K_{2V} grains form from the combination of upward traveling disturbances with a local temperature increase and downfalling matter at larger height. This combination has indeed often been proposed as grain-formation scenario [3]; CS have proven it in detail.

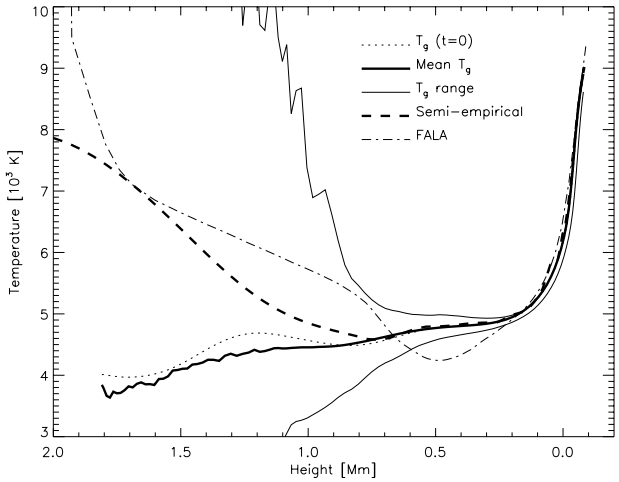

Figure 11: Temperature modeling of the solar chromosphere. FALA (dot-dashed) [39] is the newest update of the standard empirical modeling by Avrett and coworkers. The dotted curve gives the radiative-equilibrium stratification of the initial atmosphere in the CS simulation. The two thin solid curves mark the range, at each height, of the temperature variations reached during the simulation. Above $h = 1.0$ Mm the temperature varies over all the diagram but the higher values are only reached temporarily within short-duration shocks. The thick solid curve is the temporal mean. It is close to the initial stratification, implying that the shocks have not heated the mean atmosphere. The thick dashed curve is the result of modeling computed time-averaged ultraviolet continuum brightness temperatures with a best-fit hydrostatic temperature stratification. It displays an apparent chromospheric temperature rise. From [24].

7. CHROMOSPHERIC NATURE

Figure 11 displays another CS experiment [24], [41]. It compares the range of actual simulation temperatures per height with the temporal mean. It also shows the input radiative-equilibrium atmosphere, a standard semi-empirical Harvard model, and a semi-empirical model derived in Harvard fashion from the mean ultraviolet brightness temperatures delivered by the simulation. The latter has a chromospheric temperature rise much like the standard model, but the actual mean temperature does not. The latter shows that shock dissipation does not produce significant heating over the input radiative-equilibrium atmosphere during the one-hour run; the outward increase of the former is due to the nonlinear response of the Planck function to temperature increase. The high-temperature spikes in the shock fronts con-

Clapotisphere

"The extensive literature on the K_{2V} grains and related cell-interior phenomena leads us to the conclusion that bright cell grains are of hydrodynamical origin, due to oscillations that are present all over the solar surface but which produce grains only at places and moments set by pattern interference between the velocity oscillations in the K_3 layer and the evanescent wave trains of the p-mode oscillation deeper down. They remind us of what is called "clapotis" on sea charts for areas where wave interference produces waterspouts on the ocean (Dowd 1981)."

Rutten & Uitenbroek 1991

"When the crests of such waves coincide, their amplitudes combine, creating huge standing waves, much steeper than traveling waves. This phenomenon is called "clapotis". Off the northern tip of New Zealand, where major wave patterns collide in deep water, clapotis is regularly seen. The pinnacling waves formed here have so much vertical power that they can throw a laden kayak clear out of the water."

Dowd 1981

Figure 12: **Cla·po·ti·sphere** *n.* [Ol. Fr. *clapotis* from ON *klâppa* + Cl. G *sphere*], shell around star or planet with sufficient wave interaction to upset hydrostatic modelers and boaters. Ex.: 1. *CaIIK is clapotispheric.* 2. *internetwork clap* (vulg.).

tribute overly much emission, and so skew the observed mean brightness temperature to higher values than the actual mean temperature.

The nonlinear brightness sensitivity to the temperature spikes implies that modeling the quiet-Sun atmosphere by multiple components that exist side-by-side, each in hydrostatic equilibrium as if it were an extended plane-parallel atmosphere, is no longer a viable approach above $h = 1\,\mathrm{Mm}$. Not only must the network and an internetwork regimes be modeled with height-dependent geometry and pressure balances between them [42], but also the internetwork departures from hydrostatic equilibrium are sufficiently large that the dynamical variations are not to be averaged away as linear variations around a mean value. The internetwork chromosphere is inherently a *clapotisphere* (Fig. 12).

8. DISCUSSION

8.1 Phases. Skartlien *et al.* [43] determined phase relationships in various combinations from the computed I and V behavior of the Ca II lines in the CS simulation. There are parallels and discrepancies with observations [4], [44]. I don't think the discrepancies disprove the general validity of the clapotispheric picture that emerges from the simulation. Phase differences are very sensitive to the exact details of line formation and therefore to the quantitative details of the complex patterns in Fig. 10. In particular, the relationships of the Ca II infrared red lines to H & K are intricate and depend strongly on the adopted microturbulence and frequency redistribution [45].

differences between the three internetwork panels of Fig. 7. Another, yet unpublished example is that Lites and I have found that those spatio-temporal internetwork sites that display the most outstanding sequences of H_{2V} grains characteristically show deviating $V - V$ phase difference behavior for various diagnostics, tending to zero rather than propagative delays in the three-minute band. A likely explanation is that these mark downdraft sites.

In addition, phase determinations may be jeopardized by atmospheric seeing [8]. Unpublished experiments by Skartlien on the CS simulation results indicate that seeing may cause phase copying from low to high frequencies [8] which needs to be taken into account when comparing high-frequency phases between different diagnostics [46].

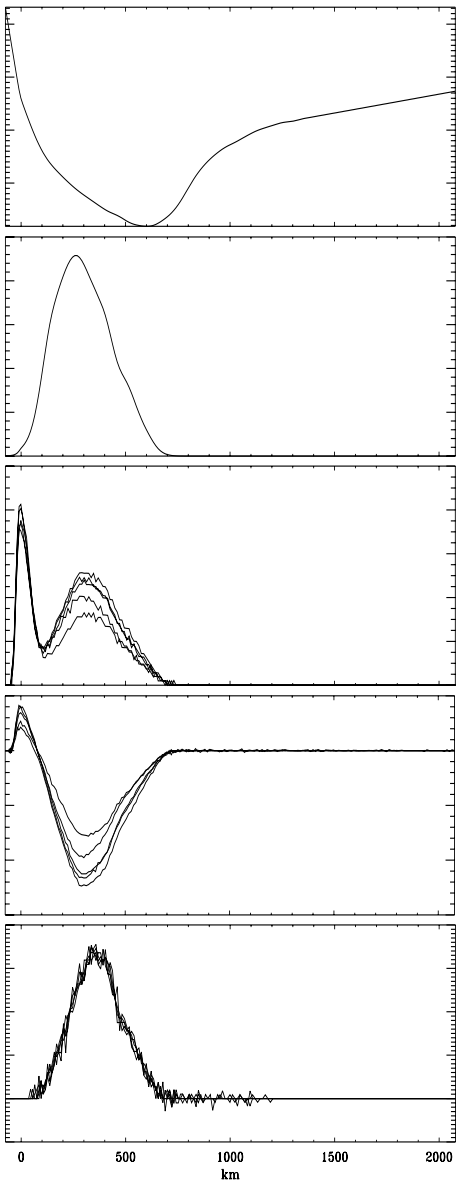

Figure 13: CO response functions from [47]. Top: VALIIIC temperature stratification [48]. Second panel: corresponding CO number density. Third panel: intensity response function. Fourth panel: line depression response function. Fifth panel: velocity response function. The response functions follow the CO concentration curve in the second panel.

8.2 CO lines. Turning the low chromosphere into a clapotisphere also explains Ayres' cool CO clouds [50], [51]. The mean temperature in Fig. 11 decreases in radiative-equilibrium manner out to $h = 1\,\mathrm{Mm}$, just as in Avrett's newest empirical model [52] from the line-

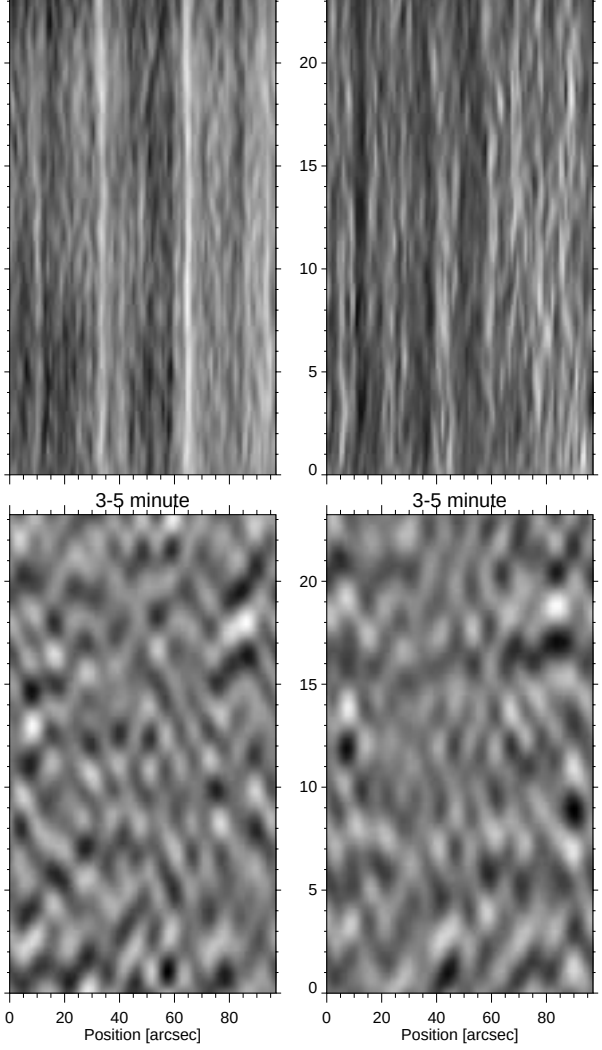

Figure 14: Filtered CO time-slices. Left: brightness temperature of the 3–2 R14 transition in the fundamental rotation-vibration CO band near 4.67 μm. Right: Dopplershift of the same line. Upper panels: low-frequency components showing convective overshoot. Lower panels: 3–5 min oscillatory components. From [49].

center brightness temperatures of ATMOS-observed CO lines across the infrared. The absence of the classical chromospheric temperature rise above $h = 500$ km adds sufficient CO opacity at sufficient low temperature to explain the observed CO limb darkening [53]. Of course, the temperature spikes in the shocks carry less weight in the infrared.

The amount of CO peaks in the upper photosphere as shown in Fig. 13 from Leifsen [47]. In a clapotisphere without mean temperature rise, CO has a longer tail of presence towards larger height but even then the CO response functions peak in the photosphere. They are wider than for atomic lines because they are set on the deep side by the dissociation of CO, not by $\exp(-\tau_\nu)$ cutoff. They are also more sensitive to temperature variations. For CO, higher temperature causes dissociation and reduces the opacity so that deeper, yet hotter layers are observed. For infrared continua and many atomic lines, the opacity and source function temperature sensitivities work against each other because temperature increase causes population increase.

The time slices in Fig. 14 from [49] prove the photospheric character of CO-line formation on the disk. The observed behavior is very similar to the behavior seen in els show convective overshoot, while the oscillation panels show upper-photosphere oscillation patterns. There are no long-lived dark clouds.

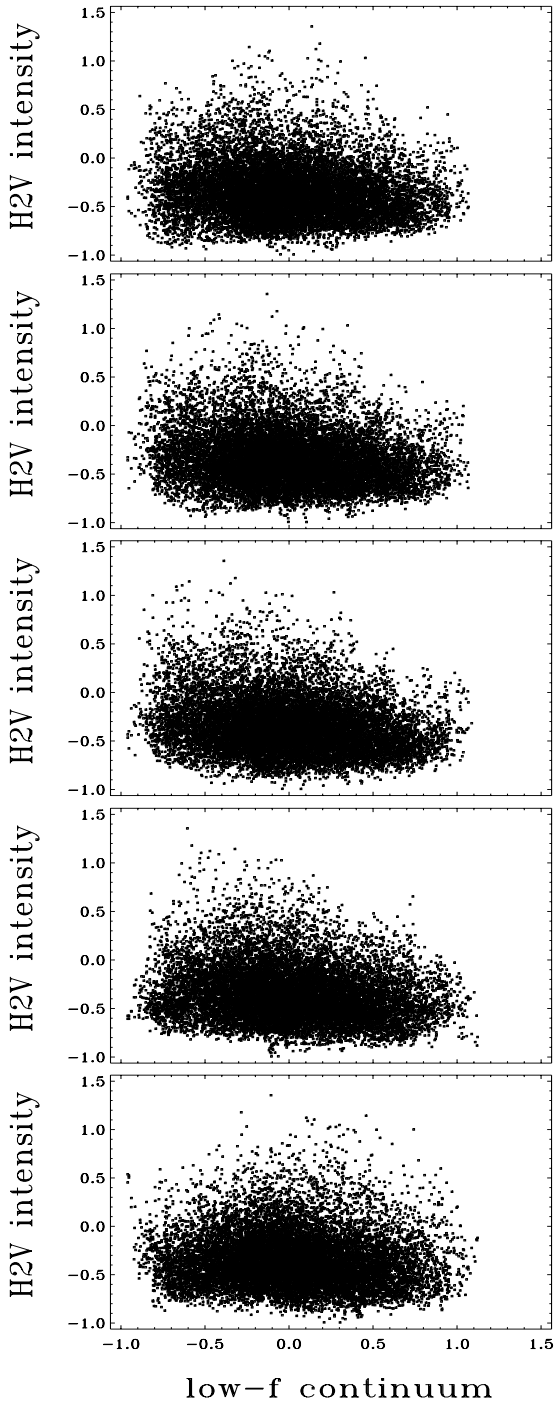

Figure 15: Scatter diagrams as in Fig. 8 for the grain-rich 116–131″ segment in Fig. 6, correlating H_{2V} intensity against the low-frequency component of the continuum intensity (granulation). The time delays between the continuum sampling and the H_{2V} sampling are from top to bottom: 0 min, 1 min, 2 min, 5 min and 10 min. Panels 3 and 4 indicate that the brightest H_{2V} grains follow 2–7 min after a dark phase of the granulation. Data of [8].

8.3 Pistons. The observations in Fig. 6 and the split-frequency simulations in Fig. 9 show that K_{2V} grains are a multi-frequency phenomenon. In the CS simulations, the (k, ω) ridge structure at photospheric levels is incorporated realistically although the simulation is only one-dimensional, because the pistoning is derived from

nated by the global p-mode oscillations and contain the p–mode interferences as present at the simulated location and time. The CS simulation is only one-dimensional, but the actual piston that they used is not: it possesses full knowledge of ambient and passing disturbances at photospheric height.

The CS piston-repeat experiment indicates that the piston behavior dictates the clapotispheric K_{2V} behavior, with time delays of 5–15 min needed to govern the higher atmosphere reproducibly. Thus, the (k, ω) ridge structure that is observed for K_{2V} intensity in Fig. 4 probably derives from the (k, ω) obedience of the underlying piston. In particular, the latter may impose the high-frequency pseudo-modes in Kumar fashion [54] as well as (k, ω) phase structure [23].

However, not all of the K_{2V} characteristics seem to be set globally. As mentioned above, the brightest grain trains possess markedly deviating phase behavior. In addition, Fig. 15 indicates that the brightest H_{2V} grains tend to follow 2–7 minutes after the underlying photosphere contained a dark intergranular lane. The body of these scatter clouds does not show correlation with the low-frequency brightness at any time lag, but the few points with the largest H_{2V} intensity favor the lefthand side in the third and fourth panels significantly. It is interesting to note that similar correlation plots of H_{2V} internetwork intensity against photospheric five-minute amplitudes at similar delays shows only a smaller effect; p–mode excursions do not seem to have the role in grain excitation that has often been attributed to them. Visual inspection of the co-spatial K_{2V} and G–band movies of Brandt *et al.* [55], [56] also indicates a correlation between the spatio-temporal patterning of H_{2V} internetwork extremes and intergranular lane morphology, rather than a correlation with photospheric p–mode pattern extrema.

This apparent intergranule connection seems to fit earlier observations of Muller and recent results of the NJIT group [57], [58] who find that high-velocity events in the photosphere, presumably contributing significantly to p–mode excitation, occur preferentially above dark sites in the granulation. Perhaps these events excite exceedingly bright K_{2V} grains as well. If that is the case, such local spatial dependences do not conform to global (k, ω) ridge structuring. They therefore seem a likely explanation for the interridge power at 6 mHz seen in Fig. 4. Its concentration to $\nu = 6$ mHz may then be interpreted as atmospheric cutoff-frequency wake response [33] to high-amplitude disturbances (at low clapotispheric temperature) rather than be attributed to the chromospheric mode invoked by [11], [12].

8.4 Internetwork fields. Sivaraman's claim [19], [20] that K_{2V} grains and their brightness are set by internetwork fields is disputed but not disproven. This apparent correlation has been attributed to *persistent flashers* [3], [55], which are loose patches of field (perhaps previously part of the network) that migrate through network interiors as if they were Lockheed corks. In fact, Brandt *et al.* [56] found that their K_{2V} flasher indeed follows the cork trajectory defined by the horizontal flows derived from granulation tracking.

Higher up, the clapotispheric role of canopies remains unclear. The Mg II h & k lines are similar to Ca II H & K but with larger opacity. Recent data [60] indicate that k_{2V} and k_{2R} peaks occur everywhere, a result that seems to require a classic chromospheric temperature rise just above the Ca II H & K formation heights. However, the complexities of Fig. 10 show that detailed modeling is also needed for these lines. In particular, Mg II h & k photons suffer yet more from resonance scattering since they lack the escape route that the Ca II infrared lines offer to H & K photons. Increased spatial smoothing may result, both radially and horizontally.

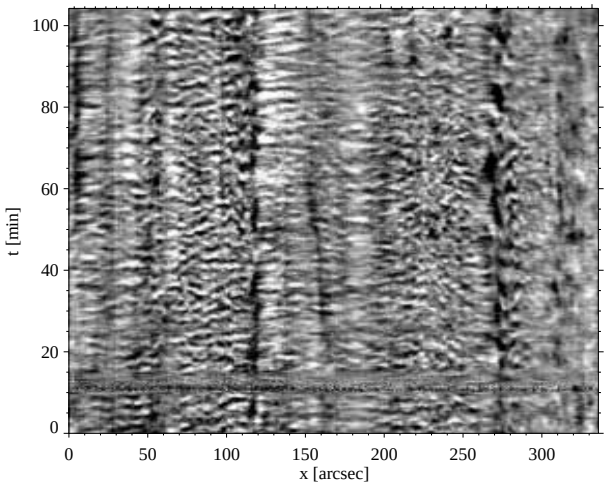

Figure 16: Doppler-shift time slice for He I 1083 nm. The slit crossed enhanced network near $x = 275''$. Over the regions $x = 60 - 100''$ and $x = 204 - 245''$ the slice displays internetwork oscillations reminiscent of Ca II H & K behavior but at appreciably smaller amplitude. The larger-scale patterning for $x = 0 - 50''$ and $x = 120 - 200''$ appears very different. From [59], courtesy of Bernhard Fleck.

He I 1083 nm doesn't offer a clearcut diagnostic either. Its Dopplershifts tend to follow H & K Dopplershifts faithfully but at smaller amplitude [8]. One may conclude that He I 1083 nm is formed below H & K or that the oscillation amplitude decreases with height, but it seems more likely that the complex formation of this line again necessitates detailed modeling rather than simple height-of-formation response estimation. The long vertical bar of brightness in the third panel of Fig. 10 upsets such interpretation already for the more simple case of Ca II H; the sensitivity of He I 1083 nm opacity to coronal radiation makes this line a much more confused diagnostic [39]. The point is proven by Fig. 16 which displays large-scale pattern variations. I wonder whether the large-scale coherency at left and in the middle portray Hα–like fibril oscillations.

8.5 Internetwork jets. Another intriguing correlation is shown in Fig. 17. It is based on HRTS–VI data and part of a manuscript-in-preparation by Hoekzema (not Hoeksema), Rutten & Cook. It shows that internetwork locations with excess C I 156 nm Dopplershift, called "chromospheric jets" in earlier analyses by Dere *et al.* [62], [63], tend to participate in a 160 nm brightness oscillation [64] – [66] with three-minute periodicity and antiphase between red jets (top curve) and blue jets (bottom curve). There is no direct one-to-one correspondence per pixel; these relations only emerge after averaging over large area. Hoekzema [61] speculates that the confusion arises from interference between upward propagating shock trains, shock-incited chromospheric undulations and f–mode waves that run transversely along canopies. The latter then produce the observed small wavelengths (1.2–1.4 Mm); the interference produces much variation; large blueshifts and redshifts result from constructive combination.

Data of much longer duration and larger spatial extent than HRTS rocket flights furnish are needed to substantiate such ideas. However, the point is that C I internetwork Dopplershifts seem related to the three-minute oscillation described above. The apparent velocities are large, but may be overestimated by the HRTS data re-

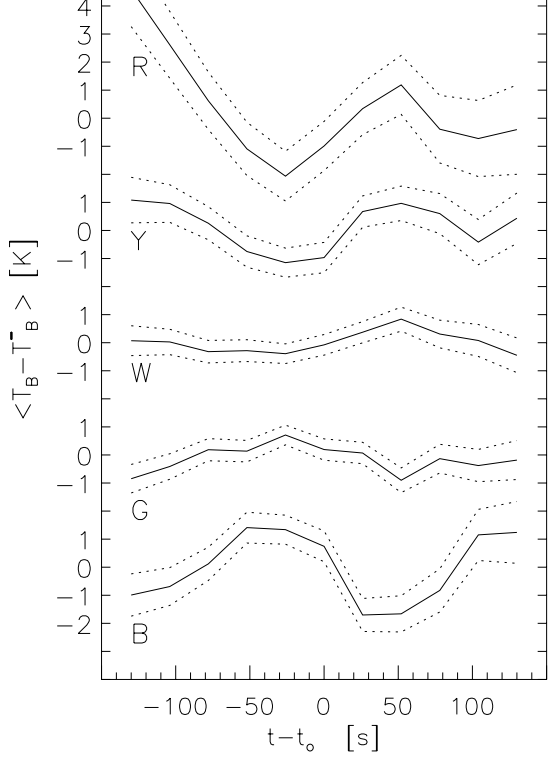

Figure 17: Statistical correlation between C I jets in the ultraviolet and the 160 nm three-minute brightness oscillation in internetwork areas. The curves are for locations with different Dopplershift of the C I 156 nm lines, split into bins ranging from redshifts above $-15\,\mathrm{km\,s^{-1}}$ (top curve, marked R) to blueshifts above $+15\,\mathrm{km\,s^{-1}}$ (bottom curve, marked B). The abscissa measures the temporal separation $t - t_0$ between the 160 nm intensity measurement and the moment t_0 at which the Dopplershift was measured. The ordinate measures the mean difference $T_\mathrm{B} - \overline{T_\mathrm{B}}$ between the instantaneous and time-averaged brightness temperature T_B per pixel, averaged over all 160 nm pixels per Dopplershift bin and per 25 s in $t - t_0$. For example, the top curve says that statistically, internetwork pixels that possess large redshift at $t = t_0$ possess brightness modulation of a few degrees in the average, with $t = t_0$ on the rising branch. Similar modulation, but with reversed sign, occurs for pixels with large blueshifts at $t = t_0$ (bottom curve). HRTS–VI data from John Cook, figure from [61].

duction procedures since they interpret displaced emission components in optically thin fashion whereas the C I lines are very thick. The H_{2V} grain in Fig. 10 sits blueshifted at twice the actual velocity at its formation height, which is the maximum upward velocity in the whole atmosphere at that moment. Similar formation of emission peaks in the ultraviolet C I lines, with substantial skewing from $\mathrm{d}\tau_\nu/\mathrm{d}\nu$ gradients caused by steep velocity gradients along the line of sight, may well enhance the apparent Dopplershifts over the actual ones. Obviously, here is work for SUMER and for C I line formation simulation.

8.6 Internetwork spicules. A final speculation concerns spicules. Conventional wisdom says that limb spicules correspond to the network mottles or fibrils seen in Hα on the disk. However, in a thoughtful review Gaizauskas [67] argues that spicules are neither mottles nor fibrils. I wonder whether they have to do with internetwork clapotis?

9. CONCLUSION

The proceedings of the 1994 Oslo Miniworkshop [5] may be compared to the proceedings of the 1975 Nice Colloa diagram equating observed and computed oscillation characteristics. In the Nice case, it was Deubner's (k, ω) diagram showing the first glimpse of the Ulrich ridges [1]. In the Oslo case, it is a Carlsson–Stein diagram with the first two columns of Fig. 9, showing that K_{2V} grains are also due to acoustic waves.

The first diagram started helioseismology. Is the second diagram of any future use? Ascribing grains to clapotispheric interference doesn't seem to make them worthwhile diagnostics. Perhaps the brightest ones are. The correlation noted in Fig. 15 suggests that these may mark high-speed downdraft sites of strong p–mode excitation.

ACKNOWLEDGEMENTS

I thank Todd Hoeksema for inviting me to give this talk and I thank Bruce Lites once again for his patience in letting me present results in such conference reviews rather than in journal papers. I am indebted to Mats Carlsson and Bernhard Fleck for providing Internet(work) figures and to Sake Hogeveen for scanning older ones. Various cooperations have been funded by NATO CRG travel grant 900229. My participation in this meeting was funded by the Leids Kerkhoven-Bosscha Fonds.

REFERENCES

[1] Ulrich, R. K.: 1970, "The five-minute oscillations on the solar surface", *Astrophys. J.* **162**, 933

[2] Deubner, F.-L.: 1975, "Observations of Low Wavenumber Nonradial Eigenmodes of the Sun", *Astron. Astrophys.* **44**, 371

[3] Rutten, R. J. and Uitenbroek, H.: 1991, "Ca II H_{2V} and K_{2V} Cell Grains", *Solar Phys.* **134**, 15

[4] Rutten, R. J.: 1994, "Internetwork Dynamics", in M. Carlsson (Ed.), *Chromospheric Dynamics*, Procs. Miniworkshop, Inst. Theor. Astrophys., Oslo, 25

[5] Carlsson, M. (Ed.): 1994, *Chromospheric Dynamics*, Proc. Mini-workshop, Inst. Theor. Astrophys., Oslo

[6] Noyes, R. W.: 1967, "Solar velocity fields", in R. N. Thomas (Ed.), *Aerodynamic Phenomena in Stellar Atmospheres*, IAU Symp. 28, Academic Press, London, 293

[7] Cram, L. E.: 1978, "High Resolution Spectroscopy of the Disk Chromosphere, VI. Power, Phase and Coherence Spectra of Atmospheric Oscillations", *Astron. Astrophys.* **70**, 345

[8] Lites, B. W., Rutten, R. J., and Thomas, J. H.: 1994, "Chromospheric oscillations", in R. J. Rutten and C. J. Schrijver (Eds.), *Solar Surface Magnetism*, NATO ASI Series C 433, Kluwer, Dordrecht, 159

[9] Deubner, F.-L., Hoffmann, J., Kossack, E., and Fleck, B.: 1994, "Non-linearities of chromospheric oscillations", in R. J. Rutten and C. J. Schrijver (Eds.), *Solar Surface Magnetism*, NATO ASI Series C433, Kluwer, Dordrecht, 155

[10] Kneer, F. and von Uexküll, M.: 1993, "Oscillations of the Sun's chromosphere. VI. K grains, resonances, and gravity waves", *Astron. Astrophys.* **274**, 585

[11] Steffens, S., Deubner, F.-L., Hofmann, J., and Fleck, B.: 1995, "Is there an atmospheric mode near 6 mhz?", these proceedings

[12] Steffens, S., Deubner, F.-L., Hofmann, J., and Fleck, B.: 1995, "On the phenomenology of K-grains", these proceedings

[13] Lites, B. W., Rutten, R. J., and Kalkofen, W.: 1993, "Dynamics of the Solar Chromosphere. I. Long-Period Network Oscillations", *Astrophys. J.* **414**, 345

1977, "High Resolution Spectroscopy of the Disk Chromosphere", *Astron. Astrophys.* **57**, 211

[15] Kneer, F. and von Uexküll, M.: 1986, "Oscillations of the Sun's chromosphere. IV. Temporal evolution of Hα profile", *Astron. Astrophys.* **155**, 178

[16] Lites, B. W.: 1994, "The dynamics of magnetic regions in the quiet chromosphere", in M. Carlsson (Ed.), *Chromospheric Dynamics*, Proc. Miniworkshop, Inst. Theor. Astrophys., Oslo, 1

[17] Hale, G. E. and Ellerman, F.: 1904, "Calcium and Hydrogen Flocculi", *Astrophys. J.* **19**, 41

[18] Cram, L. E. and Damé, L.: 1983, "High Spatial and Temporal Resolution Observations of the Solar Ca II H Line", *Astrophys. J.* **272**, 355

[19] Sivaraman, K. R. and Livingston, W. C.: 1982, "Ca II K2V Spectral Features and Their Relation to Small-Scale Photospheric Magnetic Fields", *Solar Phys.* **80**, 227

[20] Sivaraman, K. R.: 1991, "The Bright Points in the Ca II K–Line and Their Relation to the Inner Network Magnetic Structures", in P. Ulmschneider, E. Priest, and B. Rosner (Eds.), *Mechanisms of Chromospheric and Coronal Heating*, Heidelberg Conference, Springer Verlag, Berlin, 44

[21] Kulaczewski, J.: 1992, "Oscillations of the solar chromosphere", *Astron. Astrophys.* **261**, 602

[22] von Uexküll, M. and Kneer, F.: 1995, "Oscillations of the Sun's chromosphere. VII. K grains revisited", *Astron. Astrophys.* **294**, 252

[23] Hofmann, J., Deubner, F.-L., Steffens, S., and Fleck, B.: 1995, "Phase analysis of the K grain excitation pattern", these proceedings

[24] Carlsson, M. and Stein, R. F.: 1994, "Radiation shock dynamics in the solar chromosphere — results of numerical simulations", in M. Carlsson (Ed.), *Chromospheric Dynamics*, Proc. Miniworkshop, Inst. Theor. Astrophys., Oslo, 47

[25] Athay, R. G.: 1970, "Emission cores in H and K lines. V: Asymmetries in K_2 and K_3", *Solar Phys.* **11**, 347

[26] Cram, L. E.: 1972, "Multi-Component Models for the Formation of the Chromospheric Ca II Line", *Solar Phys.* **22**, 375

[27] Liu, S.-Y. and Skumanich, A.: 1974, "An Empirical Interpretation for the Time Evolution of the CaII K line", *Solar Phys.* **38**, 105

[28] Stein, R. F. and Schwartz, R. A.: 1972, "Waves in the solar atmosphere. II. Large-amplitude acoustic pulse propagation", *Astrophys. J.* **177**, 807

[29] Leibacher, J., Gouttebroze, P., and Stein, R. F.: 1982, "Solar atmopsheric dynamics. II. Nonlinear models of the photopsheric and chromospheric oscillations", *Astrophys. J.* **258**, 393

[30] Ulmschneider, P.: 1990, "Acoustic heating of stellar chromospheres and coronae", in G. Wallerstein (Ed.), *Cool Stars, Stellar Systems and the Sun*, Proc. Sixth Cambridge Workshop, Astron. Soc. Pac. Conference Series, Volume 9, 3

[31] Ulmschneider, P.: 1991, "Acoustic heating", in P. Ulmschneider, E. Priest, and B. Rosner (Eds.), *Mechanisms of Chromospheric and Coronal Heating*, Heidelberg Conference, Springer Verlag, Berlin, 328

[32] Rammacher, W. and Ulmschneider, P.: 1992, "Acoustic waves in the solar atmosphere IX. Three minute pulsations driven by shock overtaking", *Astron. Astrophys.* **253**, 586

lations of the solar chromosphere — a basic physical effect?", *Astron. Astrophys.* **250**, 235

[34] Fleck, B. and Schmitz, F.: 1993, "On the interactions of hydrodynamic shock waves in stellar atmospheres", *Astron. Astrophys.* **273**, 671

[35] Carlsson, M. and Stein, R. F.: 1992, "Non-LTE radiating acoustic shocks and CaII K2V bright points", *apj* **397**, L59

[36] Sutmann, G. and Ulmschneider, P.: 1995, "Acoustic wave propagation in the solar atmosphere I. Linear response to adiabatic wave excitation", *Astron. Astrophys.* **294**, 232

[37] Sutmann, G. and Ulmschneider, P.: 1995, "Acoustic wave propagation in the solar atmosphere II. Nonlinear response to adiabatic wave excitation", *Astron. Astrophys.* **294**, 241

[38] Beckers, J. M. and Artzner, G.: 1974, "High Resolution Spectroscopy of the Disk Chromosphere. III. Upward Moving Disturbances as Observed in the Ca II K-Line Wings", *Solar Phys.* **37**, 309

[39] Fontenla, J. M., Avrett, E. H., and Loeser, R.: 1993, "Energy balance in the solar transition region. III. Helium emission in hydrostatic, constant-abundance models with diffusion", *Astrophys. J.* **406**, 319

[40] Dowd, J.: 1981, *Sea Kayaking*, Univ. Washington Press, Seattle

[41] Carlsson, M. and Stein, R. F.: 1995, "Does a nonmagnetic solar chromosphere exist?", *apj* **440**, L29

[42] Steiner, O., Knölker, M., and Schüssler, M.: 1994, "Dynamic interaction of convection with magnetic flux sheets: first results of a new MHD code", in R. J. Rutten and C. J. Schrijver (Eds.), *Solar Surface Magnetism*, NATO ASI Series C433, Kluwer, Dordrecht, 441

[43] Skartlien, R., Carlsson, M., and Stein, R. F.: 1994, "Calcium II phase relations and chromospheric diagnostics", in M. Carlsson (Ed.), *Chromospheric Dynamics*, Proc. Miniworkshop, Inst. Theor. Astrophys., Oslo, 79

[44] Fleck, B., Deubner, F.-L., Hofmann, J., and Steffens, S.: 1994, "Wave propagation in the solar chromosphere: some new results from CaIIK, CaII8542, and HeI10830 observations", in M. Carlsson (Ed.), *Chromospheric Dynamics*, Proc. Miniworkshop, Inst. Theor. Astrophys., Oslo, 103

[45] Uitenbroek, H.: 1989, "Operator Perturbation Method for Multi–Level Line Transfer with Partial Redistribution", *Astron. Astrophys.* **213**, 360

[46] Bocchialini, K., Vial, J.-C., and Koutchmy, S.: 1994, "Dynamical properties of the chromosphere in and out of the solar magnetic network", *Astrophys. J.* **423**, L67

[47] Leifsen, T.: 1994, "Observations and simulations of time-resolved CO spectra", in M. Carlsson (Ed.), *Chromospheric Dynamics*, Proc. Miniworkshop, Inst. Theor. Astrophys., Oslo, 139

[48] Vernazza, J. E., Avrett, E. H., and Loeser, R.: 1981, "Structure of the Chromosphere. III. Models of the EUV Brightness Components of the Quiet Sun", *Astrophys. J. Suppl. Ser.* **45**, 635

[49] Uitenbroek, H. and Noyes, R. W.: 1994, "New insight in the solar T-min region from the CO lines at 4.67 micron", in M. Carlsson (Ed.), *Chromospheric Dynamics*, Proc. Miniworkshop, Inst. Theor. Astrophys., Oslo, 129

[50] Ayres, T. R.: 1981, "Thermal bifurcation in the solar outer atmosphere", *Astrophys. J.* **244**, 1064

Chromospheres", in P. Ulmschneider, E. Priest, and B. Rosner (Eds.), *Mechanisms of Chromospheric and Coronal Heating*, Heidelberg Conference, Springer Verlag, Berlin, 228

[52] Avrett, E. H.: 1995, "Two-component modeling of the solar IR CO lines", in J. R. Kuhn and M. Penn (Eds.), *Infrared Tools for Solar Astrophysics: What's Next?*, Procs. 15th NSO/Sacramento Peak Summer Workshop, Sunspot, in press

[53] Ayres, T. R. and Testerman, L.: 1981, "Fourier Transform Spectrometer Observations of Solar Carbon Monoxide. I. The Fundamental and First Overtone Bands in the Quiet Sun", *Astrophys. J.* **245**, 1124

[54] Kumar, P. and Lu, E.: 1991, "The location of the source of high-frequency solar acoustic oscillations", *Astrophys. J.* **375**, L35

[55] Brandt, P. N., Rutten, R. J., Shine, R. A., and Trujillo Bueno, J.: 1992, "Dynamics of the Quiet Solar Atmosphere: K_{2V} cell grains versus magnetic elements", in M. S. Giampapa and J. A. Bookbinder (Eds.), *Cool Stars, Stellar Systems, and the Sun*, Proc. Seventh Cambridge Workshop, Astron. Soc. Pac. Conf. Series 26, 161

[56] Brandt, P. N., Rutten, R. J., Shine, R. A., and Trujillo Bueno, J.: 1994, "On photospheric flows and chromospheric corks", in R. J. Rutten and C. J. Schrijver (Eds.), *Solar Surface Magnetism*, NATO ASI Series C 433, Kluwer, Dordrecht, 251

[57] Rimmele, T. R., Goode, P. R., Harold, E., and Stebbins, R. T.: 1995, "Dark lanes in granulation and the excitation of solar oscillations", *Astrophys. J.* **444**, L119

[58] Rimmele, T. R., Goode, P. R., Strous, L. H., and Stebbins, R. T.: 1995, "Dark lanes in granulation and the excitation of solar oscillations", these proceedings

[59] Fleck, B., Deubner, F.-L., and Hofmann, J.: 1995, "What have we learned about chromospheric oscillations from HeI 10830 Å?", in J. R. Kuhn and M. Penn (Eds.), *Infrared Tools for Solar Astrophysics: What's Next?*, Procs. 15th Summer Workshop, NSO/Sacramento Peak, Sunspot, in press

[60] Staath, E. and Lemaire, P.: 1995, "High resolution profiles of the Mg II h and Mg II k lines", *Astron. Astrophys.* **295**, 517

[61] Hoekzema, N. M.: 1994, "On C I jets and 160 nm internetwork bright points", in M. Carlsson (Ed.), *Chromospheric Dynamics*, Proc. Miniworkshop, Inst. Theor. Astrophys., Oslo, 111

[62] Dere, K. P., Bartoe, J.-D. F., and Brueckner, G. E.: 1983, "Chromospheric Jets: Possible Extreme-Ultraviolet Observations of Spicules", *Astrophys. J.* **267**, L65

[63] Dere, K. P., Bartoe, J.-D. F., and Brueckner, G. E.: 1986, "High-Resolution Telescope and Spectrograph Images of the Solar Chromosphere and Transition Zone", *Astrophys. J.* **305**, 947

[64] Foing, B. and Bonnet, R. M.: 1984, "On the Origin of the Discrete Character of the Solar Disk Brightness in the 160 nanometer Continuum", *Astrophys. J.* **279**, 848

[65] Foing, B. and Bonnet, R. M.: 1984, "Characteristic structures of the solar disc observed rocket UV filtergrams", *Astron. Astrophys.* **136**, 133

[66] Cook, J. W., Brueckner, G. E., and Bartoe, J.-D. F.: 1983, "High resolution telescope and spectrograph observations of solar fine structure in the 1600 Å region", *Astrophys. J.* **270**, L89

sphere", in R. J. Rutten and C. J. Schrijver (Eds.), *Solar Surface Magnetism*, NATO ASI Series C 433, Kluwer, Dordrecht, 133

[68] Cayrel, R. and Steinberg, M. (Eds.): 1976, *Physique des mouvements dans les atmosphères stellaires*, Colloques Internationaux du CNRS No. 250, Editions du CNRS, Paris